Evaluating the Effects of Automated Vehicle Technology on the Capacity of Freeway Weaving Sections

Gabriel Tilg [b,a], Kaidi Yang [a,*], Monica Menendez [c,d,a]

[a] *Traffic Engineering Group, Institute for Transport Planning and Systems, ETH Zurich, Switzerland*
[b] *Chair of Traffic Engineering and Control, Technical University of Munich, Germany*
[c] *Division of Engineering, New York University Abu Dhabi, United Arab Emirates*
[d] *Tandon School of Engineering, New York University, USA*

Abstract

Weaving sections, where a merge and a diverge are in close proximity, are considered as crucial bottlenecks in the highway network. Lane changes happen frequently in such sections, leading to a reduced capacity and the traffic phenomenon known as capacity drop. This paper studies how the emerging automated vehicle technology can improve the operations and increase the capacity of weaving sections. We propose an efficient yet effective multiclass hybrid model that considers two aspects of this technology in scenarios with various penetration rates: i) the potential to control the desired lane change decisions of automated vehicles, which is represented in a macroscopic manner as the distribution of lane change positions, and ii) the lower reaction time associated with automated vehicles that can reduce headways and the required gaps for lane changing maneuvers. The proposed model is successfully calibrated and validated with empirical observations from conventional vehicles at a weaving section near the city of Basel, Switzerland. It is able to replicate traffic dynamics in weaving sections including the capacity drop. This model is then applied in a simulation-based optimization framework that searches for the optimal distribution of the desired lane change positions to maximize the capacity of weaving sections. Simulation results show that by optimizing the distribution of the desired lane change positions, the capacity of the studied weaving section can increase up to 15%. The results also indicate that if the reaction time is considered as well, there is an additional combined effect that can further increase the capacity. Overall, the results show the great potential of the automated vehicle technology for increasing the capacity of weaving sections.

Keywords:
automated vehicles, traffic flow, weaving sections, multiclass hybrid model, simulation-based optimization, lane change positions

1. Introduction

A weaving section is a highway segment where an on-ramp and an off-ramp are in close proximity. The name originates from the vehicle trajectory pattern formed by drivers who change from the auxiliary lane to the highway and vice versa. Weaving sections are considered as typical bottlenecks for highway networks.

*Corresponding author.
E-mail addresses: gabriel.tilg@tum.de (Gabriel Tilg)., kaidi.yang@ivt.baug.ethz.ch (Kaidi Yang)., monica.menendez@nyu.edu (Monica Menendez).

Accepted manuscript for Transportation Research Part C: Emerging Technologies.
 DOI: https://doi.org/10.1016/j.trc.2018.09.014

Therefore, the capacity of weaving sections is of high significance for the system-wide operations of these networks.

Negative impacts on the capacity of weaving sections result from the traffic phenomenon of the capacity drop, which is widely observed and reported throughout the literature. It is defined as the decrease of the discharge flow at bottlenecks once a queue has formed upstream (Hall and Agyemang-Duah, 1991). Numerous reports show different extents of the capacity drop at merges and weaving sections, ranging normally between 3 % and 20 % (Hall and Agyemang-Duah, 1991; Cassidy and Bertini, 1999; Chung et al., 2007; Majid Sarvi, 2010; Oh and Yeo, 2012), but in some special cases up to 30% (Kerner, 2002; Yuan et al., 2014). The underlying causes for a reduced stable capacity in weaving sections include lane changes, driving behavior, high traffic densities spreading from the shoulder lane onto other freeway lanes, and the speed of vehicles in congestion (Cassidy and Rudjanakanoknad, 2005; Laval and Daganzo, 2006; Laval et al., 2007; Chung et al., 2007; Lee and Cassidy, 2009; Yuan et al., 2014). Overall, it is agreed that the cause for it is related to local traffic conditions and that lane changes are of great significance. Chen and Ahn (2018), for example, identified the two counteracting effects of lane changes that govern capacity drop: persisting voids (wasted space) and utilization of vacancies created by diverging vehicles. Recent empirical observations further suggest that the non-optimal distribution of lane change positions is of great importance for the decrease of the capacity. For example, Menendez and He (2017) and He and Menendez (2016) discovered a strongly right-skewed distribution of lane change positions (early lane change positions) in the city of Basel, Switzerland. Additionally, Lee (2008) and Sulejic et al. (2017) suggest that the concentration of lane changes in the beginning of weaving sections leads to a low capacity.

The emergence of new technologies, such as automated vehicles, facilitates the optimization and control of traffic flow (National Highway Traffic Safety Administration, 2013; Friedrich, 2015; Talebpour and Mahmassani, 2016; Yang et al., 2016, 2018). The automated vehicle technology (AVT) eliminates the influence of human factors such as the reaction time, reducing headways and the required gap for lane changing, thus potentially increasing the highway capacity. Moreover, the information provided by automated vehicles is valuable to identify the traffic states on highways, and can be used for more intricate control (Guler et al., 2014). The AVT further provides the flexibility for central traffic managers to control the motion or gap searching decisions of the vehicles and apply adequate measures to improve the operations of traffic systems (Yang et al., 2016). However, the transition from conventional to automated vehicles will not happen abruptly. Depending on the penetration rate of automated vehicles in the overall traffic stream, the effects will supposedly differ. The effects of automated vehicles at several different automation stages and penetration rates, on the capacity of the highway network of Germany were assessed by Hartmann et al. (2017). Chen et al. (2017) studied the effects of automated vehicles and conventional vehicles on highway capacity, specially under different lane policies, such as exclusive automated and/or regular vehicle lanes and mixed-use lanes. However, to the best knowledge of the authors, the specific impact of automated vehicles on weaving sections including lateral effects and considering different penetration rates still remains unknown.

The goal of this paper is to propose a systematic framework to evaluate the effects of automated vehicles on the capacity of weaving sections. The contributions are two-fold. First, we propose an efficient yet effective multi-class hybrid model to evaluate how automated vehicles can improve the operation of weaving sections regarding the effects of lane changes. Particularly, we model two aspects of the AVT: (i) the potential to control desired lane change decisions of automated vehicles, and (ii) the lower reaction times associated with automated vehicles which lead to reduced headways and shorter required gaps for lane changing maneuvers. To ensure efficiency, both aspects are characterized by direct macroscopic inputs to the proposed model. The lane changing decisions are depicted as the distribution of desired lane change positions, and the reaction times are represented by the fundamental diagrams. Moreover, we examine different application stages of such technology by considering various penetration rates. Second, the mechanism of the model enables a systematic search for an optimum distribution of desired lane change positions for a given set of input parameters in scenarios with different penetration rates. This is formulated as a simulation-based optimization problem, which is solved for each scenario using a surrogate method that is capable of finding the quasi-global optimum. Such method and the obtained distribution shed light on where to guide drivers regarding their lane changing maneuvers.

The remainder of the paper is structured as follows. Section 2 provides a short review of the related work. Section 3 describes the proposed multi-class hybrid model and shows the validation results. Section 4 explains the incorporation of the considered aspects of automated vehicles including the optimization. Subsequently, a simulation is conducted in Section 5 to show the influences of optimum desired lane change distributions and shorter reaction times on the capacity of weaving sections. Additionally, the effects of the simultaneous consideration of both aspects are analyzed. Finally, Section 6 concludes the paper and outlines possible future research.

2. Related work

Lee (2008) developed a microscopic traffic model for weaving sections based on the lane changing and car following model formulated in Menendez (2006) validated in Menendez and Daganzo (2007). Their lane changing model distinguishes between three different lane change types, i.e. free, forced, and cooperative lane changes. Inspired by the multi-lane hybrid theory (MHT) and incorporating certain ideas on the modeling of the relaxation phenomenon, Laval and Leclercq (2008) proposed a microscopic model for traffic flow at merges. Still, such microscopic models are typically computationally more complex than macroscopic models. Additionally, they involve too much stochasticity when considering the distribution of lane change positions.

Pan et al. (2016) developed a mesoscopic traffic model which is capable of reproducing traffic characteristics as heterogeneous traffic flow distributions, capacity drop and flow balancing effects. The model incorporates mandatory and discretionary lane change types. Based on the gas-kinematic theory, Ngoduy (2006) proposed a complex macroscopic multi-class model for highway weaving sections. The model is able to reproduce traffic dynamics including the capacity drop. Less intricate macroscopic models are based on the kinematic wave theory (KWT) (Lighthill and Whitham, 1955; Richards, 1956). For example, Jin (2010) introduced a lane-changing intensity parameter to model the impacts of lane changes on the traffic stream. However, this macroscopic model cannot reproduce the traffic dynamics in weaving sections including additional lanes connecting the on- and off-ramp, due to the assumption of same density across all lanes. Leclercq et al. (2011, 2016a,b) built analytical models to study the capacity drop at merges. They assumed uniformly distributed lane changes based on the empirical evidence of Daamen et al. (2010). However, another empirical study (Marczak et al., 2014) found a strongly right-skewed distribution of lane changes in weaving sections. The same conclusion was reported in Menendez and He (2017), on which data our study is based on. Therefore, we assumed that uniformly distributed lane change positions might not be adequate for weaving sections. Furthermore, Leclercq et al. (2011, 2016a) did not look at the effects of lane change positions explicitly. Such analytical models were developed in Marczak et al. (2015) to model a weaving section as a combination of merges and diverges. This model was able to reproduce the capacity drop at a weaving section in France. However, Marczak et al. (2015) took the variance of the lane change distribution as an input parameter, and thus lane change positions themselves were not explicitly considered. Chen and Ahn (2018) focused on weaving sections, next to merges and diverges. Again, the authors did not systemically test for numerous lane change position distributions but rather assumed a uniform spatial distribution and looked at three different scenarios. As such, the effects of different spatial distributions of lane changes were not explicitly examined. In Ngoduy (2006), Jin (2010) and Pan et al. (2016), the lane change positions are endogenous, and can only be calculated with model specific methods.

Sulejic et al. (2017) also considered the optimization of lane changes in weaving sections. They used a commercially available microscopic traffic flow simulation in order to test the influence of lane changing zones. Each weaving vehicle was assigned to a zone. This assignment was optimized using a swarm particle algorithm. Additionally, Tanaka et al. (2017) studied the effects of controlling 100 % of vehicles in weaving sections. The study tested different algorithms in a microscopic traffic flow simulation environment. Next to the fact that these studies are based on microscopic traffic simulation and thus not applicable for a sophisticated optimization, they examined traffic flows consisting merely of automated vehicles. Hence, the effects of mixed traffic on the capacity of the weaving section could not be investigated. Also, Sulejic et al. (2017) reported that missing vehicles cannot be avoided by their algorithm.

A multi-lane hybrid theory was proposed by Laval and Daganzo (2004, 2006) to describe the effects of lane changes on highway sections away from diverges. The authors found that the capacity drop phenomenon is strongly related to the voids created by lane-changing maneuvers in the traffic stream. The same conclusion was drawn by Laval et al. (2007), which showed that the MHT is able to reproduce the capacity drop at merges without adding calibration parameters. However, these models were not explicitly applied and tested on weaving sections.

Additionally, the possibility to model mixed traffic is not implemented simplistically in most of the described models. Only the complex continuous model of Ngoduy (2006) includes different vehicle classes. However, as mentioned before, it does not include lane change distributions as a direct input parameter. Therefore, none of the aforementioned models fit the purpose of this paper.

To address then such gap, this paper proposes a multi-class hybrid model that takes the lane change positions as a direct input and incorporates multiple vehicle classes. The proposed model builds on the MHT (Laval and Daganzo, 2006) and the multi-class cell transmission model (CTM) for mixed traffic by Levin and Boyles (2016), and includes stochastic effects. The MHT is modified to incorporate mandatory lane changes (as they are the prevailing lane change type in weaving sections), and both, conventional and automated vehicles. Therefore, the model is capable of analyzing the potential improvements that the emergence of AVT brings on weaving sections.

3. Multi-class Hybrid Model

In this section, we develop a hybrid multi-class model for weaving sections based on the original MHT and the multi-class CTM by Levin and Boyles (2016). The proposed model is then calibrated and validated with real data from a weaving section in Switzerland. For the readers' convenience, Table 1 provides an overview of the indices and the variables used in the rest of the paper.

Table 1: Nomenclature

Indices and sets		
$\mathcal{M}$		Set of vehicle classes
l, l'		Index of the lanes
$\mathcal{I}_l$		Set of cells on lane l of the weaving section
i		Index of the cells on any lane
j		Index of the time-steps
m		Index of the vehicle class
$\mathcal{N}_l$		Set of adjacent lanes to lane l
h		Index of the truncated Gaussian distribution
Variables: Macroscopic framework		
Δt	[s]	Length of time-step
Δx	[m]	Cell length
u	[m/s]	Free flow speed
κ	[veh/m]	Jam density
$w^j_{i,l}$	[m/s]	Backward wave speed for cell i at time j on lane l
$Q^j_{i,l}$	[veh/s]	Capacity of cell i at time j on lane l
$k^j_{m,i,ll'}$	[veh/m]	Density of vehicle class m in cell i at time j on lane l with ultimate destination lane l'
$S^j_{m,i,ll'}$	[veh/s]	Sending function (demand) of vehicle class m in cell i at time j on lane l with ultimate destination lane l'
$L^j_{m,i,ll'}$	[veh/s]	Lane-changing demand of vehicle class m in cell i at time j on lane l with ultimate destination lane l'

Table 1: Nomenclature (continued)

$T^j_{m,i,ll'}$	[veh/s]	Through flow demand of vehicle class m in cell i at time j on lane l with ultimate destination lane l'
$R^j_{m,i,l}$	[veh/s]	Receiving function of vehicle class m in cell i at time j on lane l
$\rho_{m,i,ll'}$	[−]	Desired probability of changing lanes for vehicle class m in cell i from lane l to lane l' (e.g. the empirical distribution for conventional vehicles)
$\pi^j_{m,i,ll'}$	[−]	Time-variant proportion of demand for vehicle class m in cell i at time j to change from lane l to lane l'
$\gamma^j_{i,l}$	[−]	Ratio by which the demand (through or lane changing) in cell i at time j on lane l is allowed to move to the next cell
$q^j_{m,i,ll'}$	[veh/s]	Actual through flow of vehicle class m in cell i at time j on lane l with ultimate destination lane l'
$\Phi^j_{m,i,ll'}$	[veh/s]	Actual lane-changing flow of vehicle class m in cell i at time j on lane l with ultimate destination lane l'
$\Psi^j_{m,i,ll'}$	[veh]	Number of lane changes of vehicle class m in cell i at time j on lane l with ultimate destination lane l'
Variables: Microscopic framework		
k_{change}	[veh/m]	Density threshold for lane change execution
$v_{\min}$	[veh/s]	Lower threshold of the particle's speed (i.e. vehicles' speed)
v_p	[m/s]	Speed of the particle (i.e. vehicle)
κ_{change}	[veh/m]	Density threshold for lane changing particles (i.e. vehicles)
α_{change}	[−]	Gap acceptance parameter that determines the density threshold for lane changing particles (i.e. vehicles)
a_0	[m/s^2]	Acceleration constant (see Allen et al. (2000))
v_{max}	[m/s]	Upper threshold of the particle's speed (see Allen et al. (2000))
b	[m/s^2]	Deceleration constant
Variables: Optimization and simulation		
H	[-]	Number of truncated Gaussian distributions
a_h	[s]	Weight of each truncated Gaussian distribution
f_h	[s]	Probability density function of each truncated Gaussian distribution
pr	[%]	Penetration rate
λ	[m]	Vehicle length
$t_{r,m}$	[s]	Reaction time associated with vehicle class m
t_{tot}	[s]	Total simulated time

This paper explicitly models the distinction between two vehicle classes, i.e. conventional and automated vehicles, considering different distributions of desired lane change positions and reaction times. The former aspect is considered, because the lane change positions are observed to be an important factor for the decreased capacity in weaving sections (Menendez and He, 2017). The latter aspect is based on the assumption that automated vehicles are able to react faster than humans, resulting in shorter headways and smaller required gaps for lane changes.

Unlike the original MHT that considers only discretionary lane changes, the proposed model focuses on mandatory lane changes, as this is the prevailing lane change type in weaving sections. For this type, the lane change positions no longer depend on the speed differences between adjacent lanes. Instead, the distribution of desired lane change positions can be regarded as exogenous and is modeled as a direct input.

This provides the possibility to optimize the lane change distribution of automated vehicles in order to maximize the capacity of the weaving section.

The proposed model consists of a macroscopic and a microscopic part. Section 3.1 describes the macroscopic framework, which is based on the KWT and its numerical representation, the CTM. The microscopic lane change algorithm is presented in Section 3.2. Section 3.3 shows the model calibration and validation with empirical data from a weaving section close to the city of Basel in Switzerland.

3.1. Macroscopic framework

This section develops the macroscopic framework of the proposed hybrid model. Both time and space are discretized as in the CTM. Each lane in the highway section is divided into a number of cells, each with a length of Δx. The time horizon is uniformly discretized into time steps, each with a duration of Δt. Here, the Courant-Friedrichs-Lewy condition $\Delta x = u\Delta t$ holds in order to ensure numerical stability, where u represents the free flow speed. In each cell, a triangular fundamental diagram is assumed with a uniform free flow speed u and jam density κ.

Denote $\mathcal{M} = \{C, A\}$ as the set of vehicle classes, indexed by m, where C represents conventional vehicles and A represents automated vehicles. Note that the framework proposed in this paper can be generalized to the cases with more than two vehicle classes. In this paper, we consider these two vehicle classes in order to evaluate the potential benefits of automated vehicles on weaving sections. We further categorize the flow and density in each cell according to the lane origin and desired ultimate destinations (hereafter abbreviated as lane ODs)[1].

It is assumed that the speed is independent of the vehicle class and the lane OD. This assumption guarantees that the conservation of each vehicle class can be treated separately. It is also assumed that the traffic densities of both classes and different lane ODs are uniformly distributed within the cells. The first-in-first-out rule applies for each cell.

The macroscopic part of the model follows the CTM and describes the traffic dynamics based on the mass conservation of each cell. It is illustrated in Figure 1, and is formulated by Equations (1)-(13).

Eq.(1) corresponds to the sending function of the KWT. It calculates the total flow $S^j_{\text{tot},i,l}$ in cell i on lane l willing to depart at time j (i.e. move to the next cell $i+1$ on any adjacent lane or lane l itself).

$$S^j_{\text{tot},i,l} = \min\left\{Q^j_{i,l}, uk^j_{\text{tot},i,l}\right\} \tag{1}$$

where the first term on the right hand side of Eq.(1) is the cell capacity $Q^j_{i,l}$. Note that the cell capacity $Q^j_{i,l}$ is not time-invariant, as it is a function of the penetration rate of the automated vehicles in cell i at time j, described by Eq.(A.1) in Appendix A. Additionally, the cell capacity is influenced by moving bottlenecks (as generated in the microscopic model). If a moving bottleneck is currently located in cell i, the corresponding capacity is adapted to the capacity given by the moving bottleneck. One example of such adaptation can be found in details in Daganzo and Laval (2005). The second part on the right hand side represents the maximum flow provided by the number of vehicles on the cell, characterized by the product of the free flow speed u and the total density $k^j_{\text{tot},i,l}$, where the total density can be represented as the sum of the densities over vehicle classes and ultimate lane destinations $l' \in \mathcal{N}_l \cup \{l\}$.

$$k^j_{\text{tot},i,l} = \sum_{l' \in \mathcal{N}_l \cup \{l\}} \sum_{m \in \mathcal{M}} k^j_{m,i,ll'} \tag{2}$$

[1]Note that the ultimate destination of a vehicle may be different from its temporary destination at a specific point. The ultimate destination is given by the vehicle's routing, and hence fixed for each vehicle and independent of the current time and the vehicle's position, whereas the temporary destination is the vehicle's real-time destination at a particular time. Consider a vehicle which desires to change lane in the end of the weaving section. The temporary destination lane of the vehicle remains the current lane until the specific point where it desires to change. At and after this specific point, the temporary destination and the ultimate destination become the same.

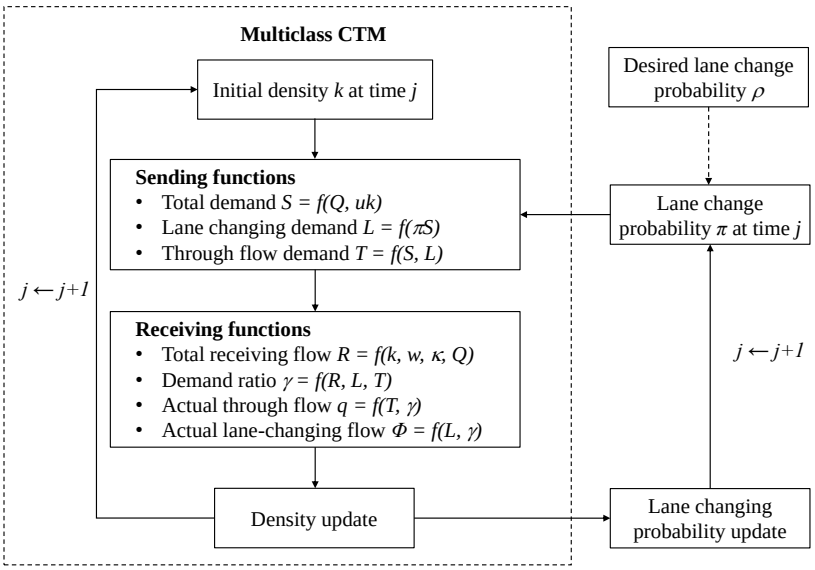

Figure 1: Macroscopic part of the modified multi-lane hybrid theory.

Given that the flow with different vehicle classes and lane ODs is uniformly distributed, the demand for each vehicle class and each lane origin l and ultimate destination $l' \in \mathcal{N}_l$, $S^j_{m,i,ll'}$, can be represented as Eq.(3).

$$S^j_{m,i,ll'} = S^j_{\text{tot},i,l} \frac{k^j_{m,i,ll'}}{k^j_{\text{tot},i,l}},\ m \in \mathcal{M},\ l' \in \mathcal{N}_l \cup \{l\} \tag{3}$$

We assume that there is a time-invariant distribution (at least for a certain period of time, e.g., several hours) of desired lane change positions for each vehicle class and each lane OD. This distribution assigns a probability for each cell i in the weaving section independently of traffic dynamics. This desired probability of changing lanes in cell i from lane l to its adjacent lane $l' \in \mathcal{N}_l$ for vehicle class m is denoted as $\rho_{m,i,ll'}$. It is derived from empirical data for conventional and manually set for automated vehicles, and is an input to the model. Note that $\forall l' \in N_l$, it holds that $l' \neq l''$, thus $\rho_{m,i,ll'}$ only applies for the vehicles that desire to change lane. Naturally, it holds that the sum of lane changing probabilities over a whole lane of the weaving section is 1 between adjacent lanes $l' \in \mathcal{N}_l$.

$$\sum_{i \in I_l} \rho_{m,i,ll'} = 1,\ m \in \mathcal{M},\ l' \in \mathcal{N}_l \tag{4}$$

These desired probabilities, however, should be adapted to the real-time traffic dynamics, i.e. flow and density, when calculating the lane changing demand. This is because the actual weaving demand in each cell is time-variant and decreases along the weaving section as more vehicles reach their final destination. For vehicle class m to change from lane l to lane $l' \in \mathcal{N}(l)$ at time j, denote $\pi^j_{m,i,ll'}$ as the time-variant probability of changing lane in cell i. The relation between $\rho_{m,i,ll'}$ and $\pi^j_{m,i,ll'}$, as well as the evolution of $\pi^j_{m,i,ll'}$, will be derived later in a recursive formula in Eq.(13). The lane-changing demand of each vehicle class and lane OD can be calculated as

$$L^j_{m,i,ll'} = \pi^j_{m,i,ll'} S^j_{m,i,ll'},\ m \in \mathcal{M},\ l' \in \mathcal{N}_l \tag{5}$$

Eq.(5) calculates the lane changing demand as a proportion of the weaving demand for the case of

$l' \in \mathcal{N}_l$. For the trivial case where the origin lane l equals the ultimate destination lane l', the lane-changing probability π is always equal zero and thus no lane changing demand exists.

The throughput flow, i.e. the flow that desires to continue on the current lane (instead of changing lanes), in cell i on lane l at time j is computed as the difference between the entire demand and the lane changing demand.

$$T^j_{m,i,ll'} = \begin{cases} S^j_{m,i,ll'} - L^j_{m,i,ll'}, & m \in \mathcal{M},\ l' \in \mathcal{N}_l \\ S^j_{m,i,ll'}, & m \in \mathcal{M},\ l' = l \end{cases} \tag{6}$$

Eq.(7) corresponds to the receiving function of the KWT. It is independent of the flow composition, but is constrained by the remaining space (the first term on the right hand side of Eq.(7) and the cell capacity $Q^j_{i+1,l}$ of cell $i+1$.

$$R^j_{i,l} = \min\left\{ w^j_{i+1,l}\left(\kappa - k^j_{\text{tot},i+1,l}\right), Q^j_{i+1,l} \right\} \tag{7}$$

where $w^j_{i+1,l}$ denotes the backward wave speed and κ the jam density in cell $i+1$ at time j. Note that $w^j_{i+1,l}$ is time-variant, as it is a function of the penetration rate of the automated vehicles in cell i at time j.

Next, we determine the ratio by which the demand (through or lane changing) is allowed to move to the next cell. This is done similarly as in Laval and Daganzo (2006) by assigning the supply to the incoming flow proportionally to the demand, given as Eq.(8).

$$\gamma^j_{i,l} = \min\left\{ 1, \frac{R^j_{i,l}}{\sum_{l' \in \mathcal{N}_l \cup \{l\}} \sum_{m \in \mathcal{M}} T^j_{m,i,ll'} + \sum_{l' \in \mathcal{N}_l} \sum_{m \in \mathcal{M}} L^j_{m,i,l'l}} \right\} \tag{8}$$

where the denominator of the second term represents the total demand in cell i on lane l at time j, which is calculated as the sum of through flow on lane l and the lane changing flow from adjacent lanes l' to lane l.

Recall that the flow of different vehicle classes and lane ODs are uniformly distributed in each cell. Therefore, the actual through flow $q^j_{m,i,ll'}$ and the actual lane changing flow $\Phi^j_{m,i,l'l}$ are calculated by multiplying the corresponding demand with the ratio $\gamma^j_{i,l}$, i.e.

$$q^j_{m,i,ll'} = T^j_{m,i,ll'} \gamma^j_{i,l},\ m \in \mathcal{M},\ l' \in \mathcal{N}_l \cup \{l\} \tag{9}$$

$$\Phi^j_{m,i,l'l} = L^j_{m,i,l'l} \gamma^j_{i,l},\ m \in \mathcal{M},\ l' \in \mathcal{N}_l \tag{10}$$

where it is assumed that the ratio $\gamma^j_{i,l}$ is split proportionally according to the demands.

The number of lane changes of class m in one time-step Δt from cell i on lane l to cell $i+1$ on lane l' is computed in Eq.(11).

$$\Psi^j_{m,i,ll'} = \Phi^j_{m,i,ll'} \Delta t,\ m \in \mathcal{M},\ l' \in \mathcal{N}_l \tag{11}$$

Then, discrete lane-changing particles are generated as outcomes from a Poisson distributed variable with mean $\Psi^j_{m,i,ll'},\ m \in \mathcal{M}$. The time-step Δt is assumed to be chosen small enough so that the likelihood of having more than one particle is negligible. This is in consensus with the model in general, since Δt should be chosen as small as possible to be able to achieve a high model accuracy (Laval and Daganzo, 2006). If there are more than one particle, they will behave the same according to the microscopic model described in Section 3.2.

The evolution of density is calculated based on the mass conservation Eq.(12). The upper part of the equation refers to that share of the flow which did not reach its final destination yet, i.e. the case $l' \in \mathcal{N}_l$. Therefore, that part which is able to change lanes during one time-step is subtracted. The lower part of Eq.(12) calculates the density for the case of $l' = l$. It includes the share of flows which comes from other lanes $l'' \neq l$ and reaches its final destination on l, thus stays on this lane further on.

$$k^{j+1}_{m,i,ll'} = \begin{cases} k^j_{m,i,ll'} - \dfrac{\Delta t}{\Delta x}(q^j_{m,i,ll'} - q^j_{m,i-1,ll'}) - \dfrac{\Delta t}{\Delta x}\Phi^j_{m,i,ll'}, & m \in \mathcal{M}, l' \in \mathcal{N}_l \\ k^j_{m,i,ll'} - \dfrac{\Delta t}{\Delta x}(q^j_{m,i,ll'} - q^j_{m,i-1,ll'}) + \dfrac{\Delta t}{\Delta x} \displaystyle\sum_{l'' \in \mathcal{N}_l} \Phi^j_{m,i-1,l''l}, & m \in \mathcal{M}, l' = l \end{cases} \tag{12}$$

Finally, we calculate the lane changing proportion in time step $j+1$. The conservation equation for the weaving flow that desires to change in cell i can be represented by Eq.(13).

$$k^{j+1}_{m,i,ll'}\pi^{j+1}_{m,i,ll'} = k^{j}_{m,i,ll'}\pi^{j}_{m,i,ll'} + \frac{\Delta t}{\Delta x}\frac{\rho_{m,i,ll'}}{\sum\limits_{i'\geq i}\rho_{m,i',ll'}}q^{j}_{m,i-1,ll'} - \frac{\Delta t}{\Delta x}\Phi^{j}_{m,i,ll'},\ m\in\mathcal{M},\ l'\in\mathcal{N}_l \tag{13}$$

where the terms $k^{j+1}_{m,i,l}\pi^{j+1}_{m,i,ll'}$ and $k^{j}_{m,i,l}\pi^{j}_{m,i,ll'}$ represent the density of such weaving flow at time $j+1$ and j, respectively. The second term on the right hand side represents the incoming density from the upstream cell. It is observed that $q^{j}_{m,i-1,ll'}$, i.e, the incoming weaving flow, only includes the vehicles willing to change in cell i and afterwards. Therefore, the proportion that desires to change lanes in cell i can be represented by the term $\rho_{m,i,ll'}/\sum_{i'\geq i}\rho_{m,i',ll'}$. The third term represents the density that has already completed the lane changing and takes the traffic state on the target lane into account. Then, $\pi^{j+1}_{m,i,ll'}$ can be solved from Eq.(13).

3.2. Microscopic framework

The previous section showed that the creation of lane-changing particles depends on the traffic state. In the current section the endogenous calculation of the trajectories of those particles including their effects on surrounding traffic is presented. This leads to a comprehensive model which reflects the mutual dependency of traffic states and lane changes by having only two additional calibration parameters compared to the original MHT.

The original MHT models discretionary lane changes by assigning a probability to each cell related to the speed differences between the origin and the destination lane. Thus, lane changes only occur when drivers would be able to increase their speed on the destination lane. However, when modeling mandatory lane changes this logic cannot be adopted. The crucial difference is that lane changes are also possible when the speed on the origin lane is higher than the one on the destination lane. Therefore, the lane-changing process must be modified.

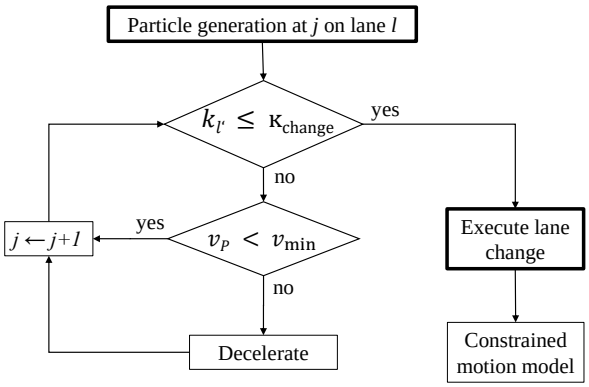

Figure 2: Microscopic lane change algorithm.

The new lane change algorithm is illustrated in Figure 2 for a particle generated at time j in cell i on lane l. For presentation simplicity, we neglect the indices of cells (i), time (j) and vehicle classes (m) of the density variables.

The intuition of the microscopic model is related to gap searching. This is achieved by comparing the density on the destination lane $k_{l'}$ with a parameter κ_{change}. More details on κ_{change} are given below. This parameter is assumed to be proportional to the amount of gaps on the destination lane l', and is therefore interpreted as the reciprocal value of the average gap size which is accepted for a lane change. Moreover, it takes into account the particle's speed v_p. The explicit relation is shown in Eq.(14).

If the density on the destination lane $k_{l'}$ is lower than κ_{change}, the lane change is executed and the particle behaves according to the constrained motion model (Laval and Daganzo, 2003). This means that after the lane change it accelerates until it reaches the maximum speed possible or the speed of traffic downstream, respectively. The acceleration and the maximum speed are chosen according to Allen et al. (2000). The speed of traffic downstream is estimated according to the fundamental diagram, which is further used to calculate the capacity restriction resulting from the moving bottlenecks. As soon as the particle's speed v_p equals the one of traffic downstream, the particle loses its state as moving bottleneck and is therefore terminated.

However, if the density condition is not met (i.e. $k_{l'} > \kappa_{\text{change}}$), the particle decelerates with the deceleration constant b from the current speed v_p to v_{min}, which is defined as the minimum speed at which drivers are looking for an appropriate $k_{l'}$ (see Figure 2). If this minimum speed is reached by the particle the gap-searching process is continued without any further deceleration. During this process the particle is acting as a moving bottleneck and thus influencing traffic flow. After the execution of the algorithm for j the time-step is updated to $j+1$ and the algorithm starts again at the evaluation of the density condition. Both, b and v_{min} are calibration parameters.

For the case where more than one particle desires to change to the same cell, the traffic flow on the destination lane is constrained by the slowest particle. Note that the influence of this case on the model's results decreases with $\Delta t \to 0$, as the probability of more than one particle changing to the same cell decreases.

In contrast to the original MHT, the lane change probability no longer refers to the probability at the time of execution, but at the time of decision for a lane change. In other words, it describes the probability that drivers decide to change lanes at a specific point. However, it is not guaranteed that they are able to execute the lane change immediately. κ_{change} is calculated as a value between 0 and κ depending on a calibration parameter α_{change}. In order to keep the algorithm as simple as possible, it is assumed that this parameter α_{change} does not depend on time and space. Tests showed that the model's accuracy is not significantly affected with such an assumption.

$$\kappa_{\text{change}} = \kappa \frac{w}{v_p + w} \alpha_{\text{change}} \tag{14}$$

where κ denotes the jam density, w the backward wave speed, v_p the speed of the particle, and α_{change} a calibration parameter.

As it is described in Appendix A, the penetration rate impacts the cell capacity Q (see Eq.(A.1)) and the backward wave speed w (see Eq.(A.2)). In other words, the backward wave speed w changes accordingly with the share of automated vehicles in the traffic stream. Therefore, Eq.(14) guarantees that κ_{change} is adapted according to the penetration rate.

3.3. Model Calibration and Validation

In this section, the model is calibrated using empirical data, and the validation results are presented. The calibration and validation of the model are based on measurements conducted within the Project WEAVE (Menendez and He, 2017) at a weaving section near the city of Basel, Switzerland. The data was measured during the entire rush hour on 5 days in October and November, 2014. The length of the studied weaving section is 500m. This weaving section has two main lanes and one auxiliary lane. It is observed that almost all (more than 92%) of the lane changes at this site are mandatory lane changes, as they either change from the main lanes to the auxiliary lane or vice versa (Menendez and He, 2017). Therefore, we build a simulated weaving section with the same layout (see Figure 3), and consider only the mandatory lane changes. This includes lane changes from lane 2 to lane 3 and vice versa as well as lane changes from lane 1 to lane 2. The latter type does not necessarily consist of mandatory lane changes only, but is included for completeness. Lane changes from lane 2 to lane 1 are not modeled as they consist merely of discretionary lane changes.

The simulation model is created using MATLAB, and calibrated with the empirical data of October 28, 2014. The lane-based fundamental diagrams are estimated based on empirical data observed at the site. These observations include lane-specific radar and video measurements, which were then aggregated and

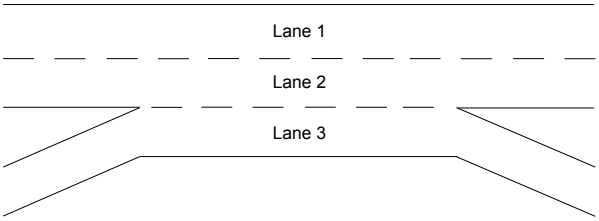

Figure 3: Schematic layout of the weaving section in Basel, Switzerland.

one fundamental diagram was defined for the whole weaving section. Furthermore, the demand is estimated based on empirical data observed at the site, too. The demand is increased step-wise to its maximum in order to load the system. The distribution of the lane change positions between lane 2 and lane 3 of the Basel data set for the calibration is shown in Figure 4a. The lane change distribution between lane 1 and lane 2 and vice versa is found to be uniform. The calibration process finds the gap acceptance parameter α_{change}, the minimum speed at which particles move $v_{\min}$ as well as the deceleration constant b to replicate the capacity drop. 10 different random seeds are considered in the calibration.

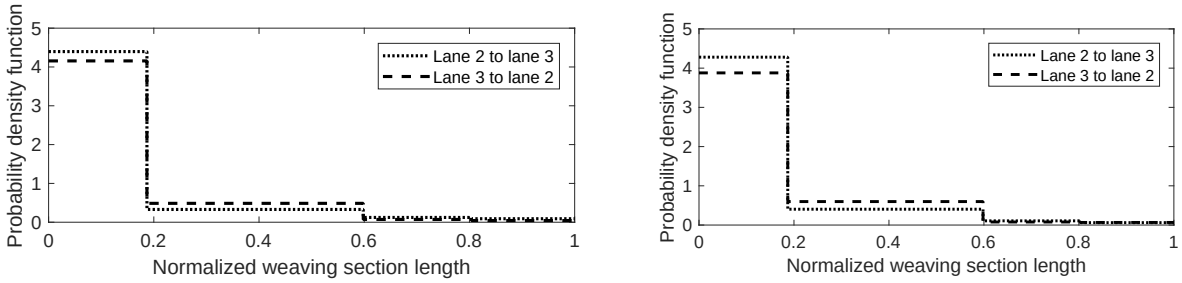

(a) PDF based on the calibration dataset.

(b) PDF based on the validation dataset.

Figure 4: Empirical probability density functions (PDF) of lane change positions.

After the successful calibration, the model is validated with another data set from the same site, which was recorded on November 3, 2014. The distribution of the lane change positions between lane 2 and lane 3 of the Basel data set for the validation is shown in Figure 4b. Again, the lane change distribution between lane 1 and lane 2 and vice versa is found to be uniform and 10 different random seeds are considered.

Figure 5 shows, using the validation data for comparison, that the proposed model can successfully reproduce the discharge rates of the weaving bottleneck and the capacity drop phenomenon for this site. The dashed line represents the cumulative departure curve from the weaving section considering the flows on all three lanes. A background flow $q = 5040\,\text{veh/hr}$ is subtracted in order to highlight the changes in flows for both analyzing the empirical and the simulated data. The solid lines are added to the figures in order to indicate the corresponding average flows.

The oblique count based on the empirical data is presented in Figure 5a. It shows the period in which the capacity drop was observed. The capacity is reduced from about $q = 5210\,\text{veh/hr}$ to a flow of $q = 4820\,\text{veh/hr}$. The difference of transient and stable capacity corresponds to a capacity drop of about $390\,\text{veh/hr}$.

Figure 5b shows the oblique count based on the simulation results. The transient capacity reaches a value of $q = 5370\,\text{veh/hr}$. It can be seen that the maximum transient flow sustains only from minute 11 to minute 17. After this point the flow decreases. The corresponding discharge rate is measured as $q = 4990\,\text{veh/hr}$. This stable capacity stays at this level during the occurrence of maximum input flow. The difference of these two values equals $380\,\text{veh/hr}$. This result is close to the empirically measured capacity

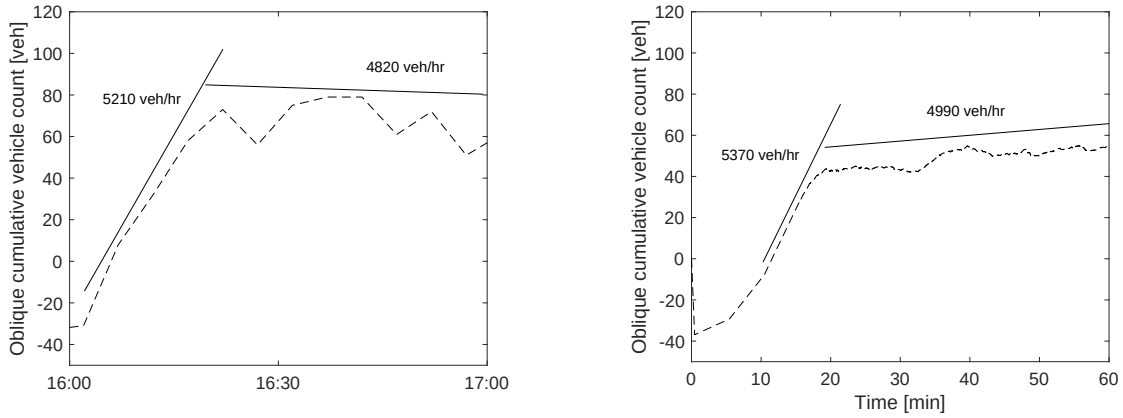

(a) Capacity drop from empirical data.

(b) Capacity drop from simulated data.

Figure 5: Oblique counts based on empirical and simulated data downstream of the weaving bottleneck. The subtracted background flow is $q = 5040$ veh/hr.

drop of 390 veh/hr. The difference in transient and stable capacities between the empirical measurements and the simulated results is 160 veh/hr and 170 veh/hr, respectively. This corresponds to relative differences of 3.1 % and 3.3 %, respectively. In both the calibration and the validation no missing vehicles are recorded, i.e. all vehicles are able to reach their ultimate destination.

4. Optimizing traffic flow using automated vehicle technology

In this section, we exploit the benefits of automated vehicles by controlling their lane change decisions to optimize traffic flow. The proposed model in Section 3 characterizes such decisions as the distribution of the desired lane change positions, which serves as a direct input to the model. Therefore, the proposed model is advantageous over the previous models (e.g. Leclercq et al., 2011, 2016b) in that it enables the possibility to optimize the lane change distribution of automated vehicles to maximize the capacity of the weaving section.

The search for the optimum distribution can be formulated as a simulation-based optimization problem. The model described in the previous Section is implemented in a simulation. For given decision variables, constraints and an objective function, an optimization is conducted based on simulation runs, which are considered as *function evaluations* in this context. The decision variables are the time-invariant desired lane changing probabilities $\rho_{m,i,ll'},\ m = A$ for automated vehicles. One constraint is that such variables should form a proper distribution, which can be mathematically represented as Eq.(15), and that all probabilities must be positive numbers Eq.(16).

$$\sum_i \rho_{m,i,ll'} = 1,\ \forall l' \in \mathcal{N}_l,\ \forall l,\ \forall m \in \mathcal{M} \tag{15}$$

$$\rho_{m,i,ll'} \geq 0,\ \forall l' \in \mathcal{N}_l,\ \forall l,\ \forall i,\ \forall m \in \mathcal{M} \tag{16}$$

Another constraint ensures that all vehicles are able to change lanes within the weaving section. This is because the capacity can be potentially increased by having fewer vehicles changing lanes within the weaving section. Therefore, it is important to rule out such type of solutions. However, as the proposed model is highly non-linear and stochastic, we cannot give a theoretical guarantee for this constraint. Instead, we sample a set of random seeds, and require that this constraint is satisfied over this sampled set.

The objective function is taken as the mean value of the stable capacity of the weaving bottleneck, which can be again approximated by the average over the sampled set of random seeds. The stable capacity is

calculated as the minimum moving average of the discharge rate at the end of the weaving section considering only the flows occurring after the capacity drop happened. For the moving average a range of 20 minutes is considered.

This formulation as described above is non-parametric, i.e. it optimizes the probability of each possible lane changing position, instead of the parameters in a given distribution. This problem can be solved using simulation-based optimization techniques, such as the stochastic approximation (e.g. Simultaneous Perturbation Stochastic Approximation, Spall, 1992) and surrogate models (also known as response surface methods or metamodels) (e.g. Regis and Shoemaker, 2007). However, the large number of decision variables, the several hundred function evaluations needed, and the randomness in the system together lead to a high computational cost for the optimization. Additionally, it is likely that these methods may provide unsatisfying and unstable solutions for the global problem. Moreover, as no smoothness constraints are imposed, the obtained distribution may have unexpected oscillations. Therefore, we add a parametric constraint to the optimization problem to search for a quasi-optimal solution by approximating the lane change distribution as a truncated Gaussian mixture distribution, i.e.

$$\rho_{m,i,ll'} = \sum_{h=1}^{H} a_{h,m,ll'} f_{h,m,ll'}(i) \tag{17}$$

where H denotes the number of truncated Gaussian distributions, $f_{h,m,ll'}(\cdot)$ the spatial probability density function that assigns each cell a probability of each truncated Gaussian distribution, and $a_{h,m,ll'}$ the corresponding weight. We also require that $\sum_{h=1}^{H} a_{h,m,ll'} = 1$ to ensure that Eq.(15) holds. Eq.(15) - (17) refer to the lane changing distribution related to both lane changing flow directions. That means that different distributions for both flow directions can be examined. With the parametric approximation, we aim to optimize the mean, standard deviation, and weight of each Gaussian distribution. The selection of the truncated Gaussian mixture distribution allows for an approximation of any distribution. In other words, it keeps the optimization as generic as possible.

To this end, we apply surrogate models to conduct the simulation-based optimization. The applicability of such models for the transportation field was e.g. shown in He (2014). The model described in Section 3 cannot be solved analytically and thus must be evaluated in a simulation. Compared to analytic solutions, this simulation is considered as computationally expensive. Generally, the exact mathematical relation between the input of a simulation and its output cannot be stated explicitly. Thus, such functional relationships can be considered to be of a black-box type. For computationally expensive black-box optimization problems, the use of surrogate models is expedient (Müller, 2014a,b). The reason is explained in the following. Surrogate models build an approximative and continuous surface based on a number of initial evaluations of the original expensive function. The next most promising candidate for a function evaluation is then chosen based on this response surface, which evaluation is substantially less computationally expensive than the original function. Therefore, surrogate models require less function evaluations for computationally expensive black-box functions than other algorithms like e.g. the particle swarm method (Müller and Shoemaker, 2014). The optimization of lane change positions is of such a computationally expensive black-box type, and thus the use of surrogate models seems to be an appropriate choice. Additionally, this method is able to handle stochasticity and to find the global optimum.

The schematic optimization framework of this paper is shown in Figure 6. The input for the optimization is generated with an experimental design. Generally, the purpose of experimental design methods is to maximize the outcome of information for a limited number of initial points and a high number of possible parameter combinations. In other words, by using an appropriate experimental design one is able to limit the total number of function evaluations needed in order to reach the optimum. More details and examples for different types of experimental design methods can be found in Morris and Mitchell (1995), Montgomery (2017) and Koehler and Owen (1996). To generate initial points for the optimization conducted in this paper, a Sobol quasi-random sequence is applied, which typically provides a faster convergence speed (Ge et al., 2014, 2015; Ge and Menendez, 2017).

After the expensive function evaluations at the initial points are completed, a surrogate model is fitted to the data. The surrogate model used in this paper is the radial basis function (RBF). This choice is based on

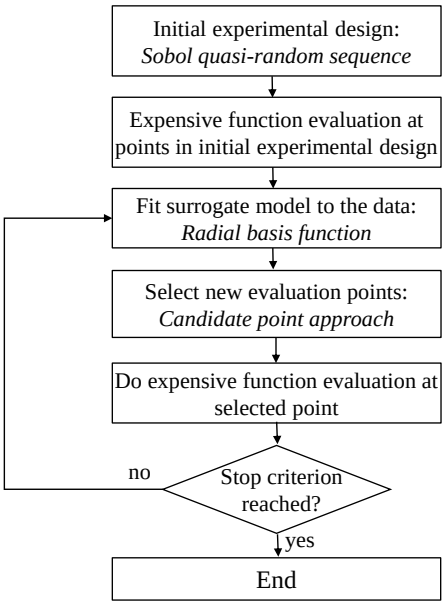

Figure 6: Schematic optimization framework based on Müller (2014a).

the findings of Müller and Shoemaker (2014), which examined different surrogate models including Kriging methods and RBF methods. They showed that the RBF method leads to the best results in all examined scenarios. Other studies have confirmed the convincing properties of RBF in terms of convergence (Björkman and Holmström, 2000; Gutmann, 2001; Regis and Shoemaker, 2005; Zhou et al., 2013). Additionally, we conducted numerical tests which showed that the conclusion drawn in Müller and Shoemaker (2014) also applies to the optimization problem tackled here.

Based on this approximative response surface, the next point is selected where the original function is evaluated. The strategy for selecting the next sample point is chosen as the candidate point approach (Regis and Shoemaker, 2007). This iterative method selects one point out of many randomly generated points on the response surface, which are called candidate points. The selection is based on two criteria. First, the estimated function evaluation should be low, since the goal is a minimization. Second, the new candidate should have a far distance from the last one. This facilitates a global search. When the candidate point is selected, the expensive original function is evaluated. Subsequently, the response surface is updated and new candidate points are defined. This process continues until the convergence criteria are met (e.g. a pre-defined minimum change of capacity of the weaving section).

This framework enables to systematically search for an optimum lane change distribution. All constraints are considered and a maximum capacity can be found for any given penetration rate of automated vehicles. Thus, the corresponding effects of the found desired lane change distribution can be quantified.

5. Evaluation of the impact of automated vehicle technology

In this section, we apply the proposed model to evaluate the impact of the AVT on the capacity of weaving sections under various penetration rates. Two types of scenarios are considered based on whether the difference in reaction times for both vehicle classes is taken into account. In the first type of scenarios, we assume that reaction times associated to automated vehicles are equal to the ones associated to conventional vehicles, i.e. there is a unique fundamental diagram independent of the penetration rate. These scenarios illustrate the benefits of optimizing the lane change decisions for a certain percentage of vehicles. In the second type of scenarios, we assume a shorter reaction time for automated vehicles. The fundamental

diagrams in such scenarios are given in Levin and Boyles (2016), and briefly described in Appendix A. These scenarios demonstrate how the benefits of optimizing the lane change distribution are affected by the reduction of reaction times. The simulation settings are described in Section 5.1. In Section 5.2 and Section 5.3, the impact of AVT is evaluated in the aforementioned two types of scenarios, under various penetration rates. Section 5.4 examines the combination effect which occurs when both, optimized lane change positions and reduced reaction times associated with automated vehicles are considered. Based on these subsections, Section 5.5 shows a lower and an upper bound for the effects of AVT on the capacity of weaving sections.

5.1. Simulation setup

To gain insights into the effects of AVT on the capacity of weaving sections, we simulate a weaving section with two lanes, a main lane and an auxiliary lane. The length of the weaving section is 500 m, as in the WEAVE project. Note that we consider the two-lane weaving section for presentation simplicity. The proposed model and optimization method can be applied to scenarios with multiple lanes. The simulated weaving section is shown in Figure 7 where four types of flows are considered. The demand is set to maximum in order to represent traffic during rush hours.

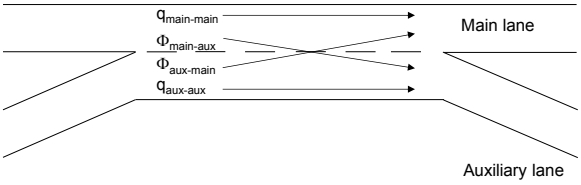

Figure 7: Layout of the simulated weaving section. The flows are the weaving flow (q) and the non-weaving flow (Φ) with different origins and destinations. The main lane is denoted as *main*, and the auxiliary lane is denoted as *aux*.

In this paper, the conventional vehicles are assumed to behave according to empirical observations made in the WEAVE project Menendez and He (2017), presented in Section 3.3. However, the proposed model is not limited to that data. Any empirical input parameter configuration for conventional vehicles is possible. The input parameters applied in the simulation correspond to the ones of the validation dataset. The fundamental diagram parameters and the three calibration parameters are thus based on empirical data. Similarly, the vehicle length and the reaction time associated to conventional vehicles are chosen to represent the empirical data. The reaction time associated to automated vehicles is chosen according to Levin and Boyles (2016). The initial weaving ratio is set to 0.7. This means that 70 % of the incoming flow on each lane has the other lane as ultimate destination. This value is set equally for both lanes in order to decrease the effect of the weaving ratio on the capacity of the weaving section. This helps to highlight the effects of lane change positions. The acceleration constant and the maximum possible speed which have to be specified for the constrained motion model (see Section 3.2), are selected as suggested in Allen et al. (2000). Note that the maximum speed v_{max} does relate to the mechanical properties of vehicles and can then be higher than the free flow speed u. More examples can be found in Laval and Daganzo (2006) and in Laval and Leclercq (2008). The time-step length as well as the total simulated time for each scenario are chosen based on numerical tests which showed that these values lead to the best trade-off between accuracy and computational cost. The parameters are summarized in Table 2.

Each evaluation analysis is conducted for six scenarios with different penetration rates starting at 0 % and ending at 100 % with an increment of 20 %. For each scenario, the optimization process described in Section 4 is implemented by using and adapting the MATLAB toolbox developed by Müller (2014b), which is based on Müller and Piché (2011), Müller et al. (2013, 2014) and Müller and Shoemaker (2014). To reach a reasonable compromise between computational complexity and optimality, we optimize a Gaussian mixture distribution as the weighted sum of 3 Gaussian distributions. The result of one simulation run is influenced by the Poisson distributed temporal generation of particles. To account for that, the objective function of each scenario is approximated by the average of 10 random seeds. Numerical tests have shown

Table 2: Simulation parameters.

Label	Parameter	Unit	Value
Free flow speed	u	[m/s]	22.22
Jam density	κ	[veh/m]	0.125
Penetration rate	pr	[%]	0-100
Gap acceptance parameter	α_{change}	[-]	0.96
Lower threshold of the particle's speed	$v_{\min}$	[m/s]	8.33
Deceleration constant	b	[m/s^2]	2
Vehicle length	λ	[m]	8
Reaction time associated with conventional vehicles	t_r, c	[s]	1.44
Reaction time associated with automated vehicles	t_r, a	[s]	0.5
Acceleration constant	a_0	[m/s^2]	4
Upper threshold of the particle's speed	v_{max}	[m/s]	38.89
Length of time-step	Δt	[s]	0.25
Total simulated time	t_{tot}	[s]	3600
Number of truncated Gaussian distributions	H	[-]	3

that the choice of 10 different random seeds represents a good compromise between computational cost and robustness of the result. Solutions leading to non-executed lane changes are largely penalized while looking for the optimum. This procedure represents a conservative lane changing behavior, since aggressive lane changing at the end of the weaving section is not explicitly considered. It is assumed that a conservative driving behavior of automated vehicles is expedient in mixed traffic, e.g. due to traffic safety.

The initial design consists of 45 function evaluations and is created based on the Sobol quasi-random sequences. Based on the results of these computationally expensive function evaluations, the surrogate model creates a approximative response surface. For each scenario, 300 additional function evaluations are run to reach a satisfying convergence, i.e. if the change of the objective value is negligibly small (the change of capacity is less than 5 veh/hr), which corresponds to the stop criterion (see Figure 6).

With the optimized lane change distribution, we further evaluate each scenario with a set of 50 random seeds. Note that more random seeds are chosen for evaluation than for optimization. This is to validate the optimized lane change distribution with a wider range of situations. For each scenario, the average capacity and average missing rate (i.e. the percentage of vehicles that fail to change lane within the weaving section) are recorded.

5.2. Impact of AVT: optimized lane change positions assuming same reaction times

In this subsection, we study the effects of optimizing the lane change positions. The headways associated to both vehicles classes are assumed to be based on the human reaction times (see Table 2). The capacity and backward wave speed can be calculated according to Appendix A as 2000 veh/hr and 20.0 km/hr, respectively. Conventional vehicles change lanes according to the empirically observed distribution in the validation data (see Figure 4b).

The simulation results are presented in Figure 8. The y-axis depicts the capacity in vehicles per hour averaged across lanes. The x-axis shows the penetration rate of automated vehicles in the traffic stream in per cent. The actual capacity is depicted as a dashed line while the maximum capacity is shown as a solid line. Additionally, error bars are added to indicate the values of the 95 % confidence interval of the actual capacity. The theoretically maximum possible capacity is shown as a reference value for the actual capacity. It corresponds to the capacity of the fundamental diagram. The values of the maximum capacity are constant since they are not influenced by the share of automated vehicles in the scenarios evaluated in these scenarios.

The results show that the positions of lane changes alone have a significant impact on the actual discharge rate of the simulated weaving section. The optimization method is able to find the optimal desired

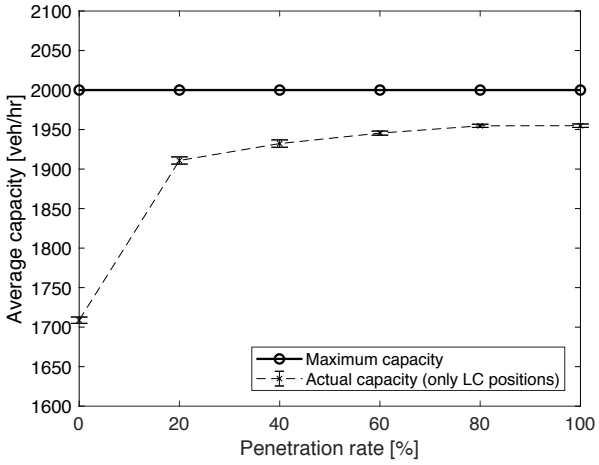

Figure 8: Capacity for several penetration rates of AVT considering optimized lane change positions.

distribution for automated vehicles which maximizes the capacity for each penetration rate. Thereby, the actual capacity can be increased from about 1700 veh/hr with no automated vehicles in the traffic stream up to about 1950 veh/hr with only automated vehicles in the weaving section. These values are averaged across lanes. The increase compared to the base case of 1700 veh/hr is about 15 %. The improvement becomes more evident, when it is considered in relation to the maximum possible improvement of 300 veh/hr. Then, one can see that about 83 % of the maximum theoretically achievable improvement is reached by looking for an optimum lane change distribution. Moreover, it can be seen that the marginal benefits of more automated vehicles decrease with an increase in penetration rate. Additionally, only one missing vehicle occurs within the tested 50 runs at the scenario with a penetration rate of 100 %. None of the evaluation runs for the other scenarios show any missing vehicles.

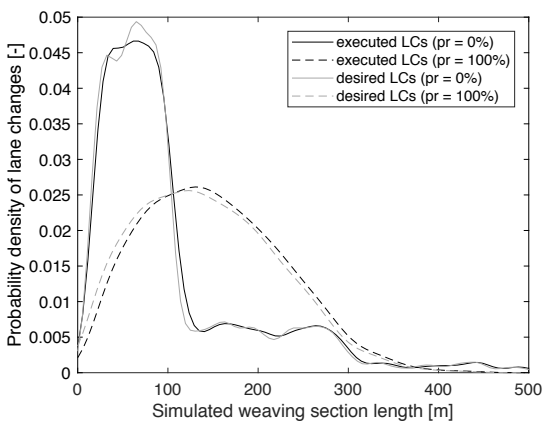

(a) Input and output lane change distributions.

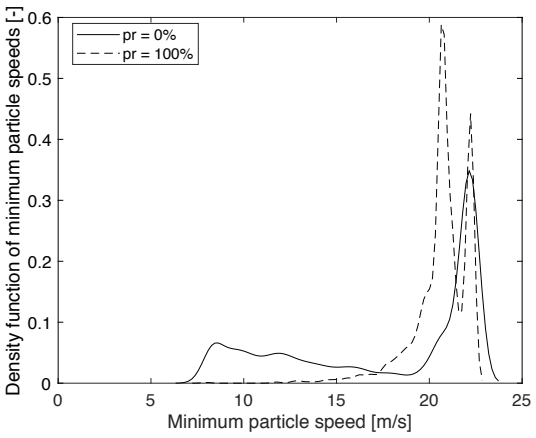

(b) Minimum speed of particles.

Figure 9: Performance comparison for penetration rates of 0 % and 100 % of automated vehicles.

In order to understand some underlying reasons for the aforementioned observations, the performance of the weaving section considering different penetration rates is examined in detail. Figure 9a illustrates the input (gray lines) and the output (black lines) distribution of lane change positions for two extreme scenarios (0 and 100 % penetration rate). The gray lines correspond to the desired lane change positions and the black lines to the distribution of executed lane changes. The recorded positions are shown as probability density

function across the simulated weaving section. The underlying data is given in a discrete form, i.e. the number of executed lane changes per cell is recorded. However, the curves are smoothed for presentation purposes. The distribution of executed lane change positions from the auxiliary lane to the main lane and vice versa do not substantially differ. Thus, Figure 9a shows the average lane change positions for both lane changing flows. The solid line depicts the lane changes for a 0 % penetration rate, while the dashed line illustrates the distribution for a 100 % penetration rate.

Analyzing the output distributions, Figure 9a is consistent with our intuition, and suggests that a slightly right-skewed distribution with the mean in the first third of the weaving section leads to a higher capacity. This outcome might result from the fact that a less concentrated distribution of lane changes in general leads to smaller voids in the traffic stream Menendez and Daganzo (2007). The higher concentration of lane changes in the beginning of the section might be reasoned by the fact that voids created in the beginning of the weaving section have a higher chance of being filled by other lane-changing vehicles later on, when compared to voids created towards the end of the section.

Lane changing particles are following the algorithm described in Section 3.2 in order to check if they are able to change lanes. Since the density conditions might not be met immediately for all particles, the distribution of executed and desired lane change positions might deviate from each other. However, the distribution of executed lane change positions for both scenarios do not deviate much from the distribution of the desired lane change positions. Figure 9b shows the distributions of minimum particle speeds for both scenarios. These minimum speeds relate to the looking-for-gap state of particles, since particles accelerate after they successfully change lanes until their termination. The figure reveals that in the case of 100 % automated vehicles, the minimum speeds of particles are much higher than for the case with conventional vehicles only. Thus, lane changing vehicles spend less time accelerating and the resulting voids in the traffic flow are smaller. Ultimately, this leads to a higher capacity.

Notice, however, that the real optimum is not known. Hence, the quality of the found solutions can only be estimated. Given the high number of function evaluations and the small changes of the objective value,we can reasonably assume that the found optimum is near to the real one. Additionally, for the scenario of 100 % automated vehicles, assuming the same reaction time which is associated to conventional vehicles, the solution is very close to the theoretical maximum capacity. The latter value serves as an upper bound for the optimization in this scenario. Assuming that the optimization results have a similar quality in all scenarios, this result is another hint that the found optimum is close to the real one.

5.3. Impact of AVT: optimized lane change positions assuming reduced reaction times

This subsection studies the impact of optimizing the lane change positions of the AVT considering reduced reaction times associated to automated vehicles. To highlight the potential of both AVT aspects in terms of increasing the capacity, three curves are shown in Figure 10. The axes correspond to the ones of Figure 8 in Section 5.2.

First, and similar to Figure 8, the maximum capacity is plotted. Again, the values depend on the fundamental diagram. However, the fundamental diagram depends on the penetration rate as described in Appendix A since we are considering different reaction times associated to the two vehicle classes. Thus, the maximum capacity increases with a growing penetration rate as shown in Figure 10 as solid line.

Second, the actual capacity is calculated for the case that automated vehicles have reduced reaction times. The impact of the share of automated vehicles on the capacity and backward wave speed at each position of the numerical grid of the simulation is explained in Appendix A. In order to understand the effects of reduced reaction times alone, the distribution of lane change positions is assumed to be equal to the empirically observed distribution in the validation data (see Figure 4b) for both vehicle classes. Therefore, the penetration rate in each cell stays the same throughout the whole highway section. Thus, the fundamental diagram is modified equally in all cells according to Levin and Boyles (2016). Ultimately, the increase of the penetration rate leads to an increase of the actual capacity of the weaving section in these scenarios. The results are illustrated as dotted line in Figure 10. It can be seen that similar to the maximum capacity, also the actual capacity grows from 1700 veh/hr to about 3300 veh/hr when only reduced reaction times are considered. These values serve as base to derive the combination effect that occurs when both

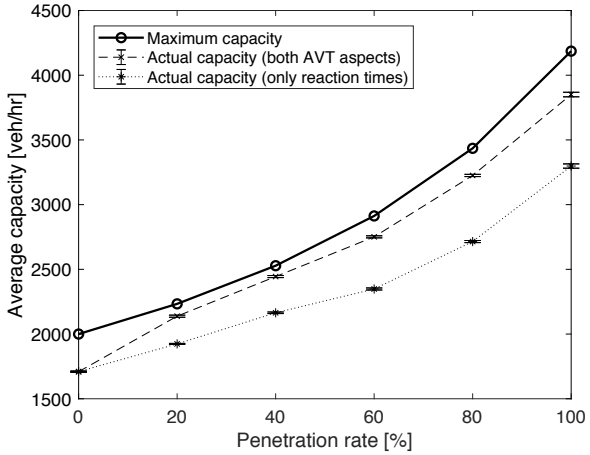

Figure 10: Capacity for several penetration rates considering different reaction times.

AVT aspects are combined (see Section 5.4). Error bars indicate the range of the 95 % confidence interval of the recorded capacities. However, the range seems to be negligibly small.

Third, the actual capacity is calculated for the case that automated vehicles have reduced reaction times and their desired lane change positions can be controlled. For each examined penetration rate the lane change distribution is optimized as described in Section 4. Additionally, the reduced reaction time associated to automated vehicles is taken into account. This leads to the fact that the fundamental diagram can vary across each position in the time-space area. As expected, the capacity can be additionally improved, as illustrated by the dashed line in Figure 10. The actual capacity increases from 1700 veh/hr to about 3800 veh/hr, which is an additional 500 veh/hr more than the potential of reduced reaction times only. As before, error bars indicate the range of the 95 %-confidence interval of the measured capacities which seem to be negligibly small again. The recorded actual capacities are close to the maximum possible capacities and show the potential improvement of automated vehicles in weaving sections.

Similar to Section 5.2, the missing vehicles were recorded. A total of two missing vehicles occurs within the tested 50 runs at a penetration rate of 100 % when both AVT aspects are considered. All other evaluation runs including those when only reduced reaction times are considered do not show any missing vehicles.

Another way of comparing the latter two curves is to set them in relation to the maximum capacity, as shown in Figure 11. This describes the capacity reduction for each scenario, which is distinguished from the capacity drop. The latter one is the ratio of the transient and the stable capacity, whereas the capacity reduction shown here is the stable capacity compared to the theoretically potential of the capacity based on the fundamental diagram. In contrary to the capacity reduction, the capacity drop depends thus also on the transient capacity which might differ from case to case and is influenced by stochasticity. Therefore, the capacity reduction is chosen in order to create comparability between the two cases in terms of considered AVT aspects.

The dashed line illustrates the capacity reduction occurring when only reduced reaction times are considered. It can be seen that the curve stays at more or less the same level and strongly increases from 40 % to 60 % penetration rate and slightly afterwards. This general behavior might be explained as follows. Due to the increasing maximum capacity, which follows from the reduced reaction times associated to automated vehicles, it is not surprising that the average capacity generally increases as well. The growing capacity reduction, on the other hand, seems to be counter-intuitive at first glance. In the simulation studies the demand was adapted according to the capacity. Thus, a growing capacity leads to a higher flow and therefore also to a higher number of lane changes in the weaving section. According to the modified MHT, lane changing vehicles might create voids in the traffic stream, and more lane changes typically lead to more voids in the traffic stream. However, those voids are not filled as fast as they are created as the free flow

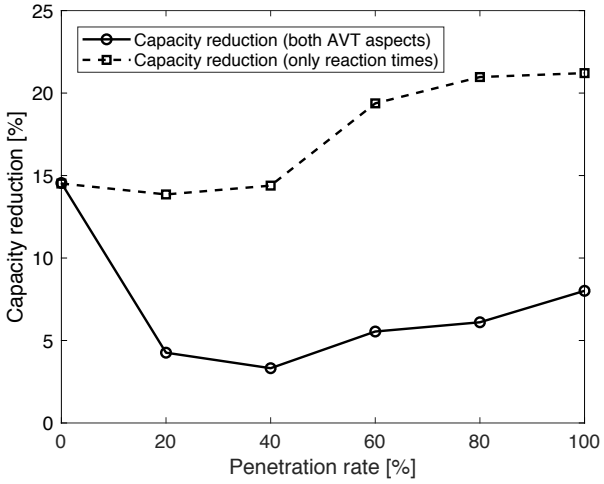

Figure 11: Capacity reduction considering both aspects of AVT and shorter reaction times only.

speed and acceleration rate are independent of the vehicle class. Thus, a higher amount of lane changing automated vehicles leads to more voids in the traffic flow and consequently to a higher capacity reduction. The fact that this increase occurs mainly after a penetration rate of 40 % might result from the specific shape of the lane change distribution. As shown by the solid line, which corresponds to the case where both AVT aspects are considered, the capacity reduction relies strongly on the lane change distribution. For the case of considering both AVT aspects simultaneously the increase of the capacity reduction is much lower. The difference shows the potential of controlling the desired lane change positions of automated vehicles. The impact of lane change positions on the capacity of the simulated weaving sections gains more importance when the total traffic volume increases. This shows that there exists a combination effect between those two aspects.

Summing up, the results presented in Figure 10 and Figure 11 indicate the high potential of controlling the desired lane change positions in order to decrease the capacity reduction, i.e. increase the actual capacity of the weaving section. Additionally, the results indicate the existence of a combination effect when both AVT aspects are considered.

5.4. Combination effects between the lane change positions and the reaction time

In this subsection, we further investigate the benefits of optimizing the lane change positions when considering the difference in reaction times associated to both vehicle classes.

The previous subsections investigated the actual capacity improvements for three different cases: (i) the controllability of desired lane change positions ($E_{LC}(pr)$), (ii) the reduced reaction times associated with automated vehicles ($E_{RT}(pr)$) and (iii) the combination of both AVT effects ($E_{tot}(pr)$). For each penetration rate the different effects in terms of actual capacity increases are recorded and listed in Table 3. The last column of Table 3 represents the combination effects, explained as follows.

The investigation of these numerical results shows the existence of a positive combination effect. This effect can be modeled as Eq.(18)

$$E_{tot}(pr) = \beta_{LC} E_{LC}(pr) + \beta_{RT} E_{RT}(pr) + \beta_{LC}\beta_{RT} E_{CO}(pr) \tag{18}$$

where $E_{tot}(pr)$, $E_{LC}(pr)$, $E_{RT}(pr)$, $E_{CO}(pr)$ represent the total effect, the effect of the lane change positions, the effect of the reduced reaction time, and the combination effect between those two aspects in scenarios with penetration rate pr. The coefficients β_{LC} and β_{RT} take only values of 0 or 1 depending on whether the corresponding aspect is considered.

Table 3: Actual capacity improvements for all scenarios.

Penetration rate (pr) [%]	Total effect $E_{tot}(pr)$ [veh/hr]	Lane change position effect $E_{LC}(pr)$ [veh/hr]	Reaction time effect $E_{RT}(pr)$ [veh/hr]	Combination effect E_{CO} [veh/hr]
0	0	0	0	0
20	430	200	215	15
40	735	225	455	55
60	1040	235	635	170
80	1515	245	1005	265
100	2140	245	1575	320

The combination effect is understood as the extra benefits obtained from the optimization of the lane change distribution as the reaction time associated to automated vehicles decreases. It can be seen that the combination effect is always positive, and increases strictly monotonically with the penetration rate. This suggests that the improvement in terms of actual discharge flow is higher when considering both aspects simultaneously than when we simply sum the improvements of both aspects considered separately. Therefore, this confirms that the distribution of desired lane changes is of growing importance when the penetration rate of automated vehicles increases.

5.5. Lower and Upper bound for the effects of an optimized lane change distribution

This investigation shows that the effects of optimizing the lane changing positions for varying reaction times associated with automated vehicles differ. Based on that, a lower and an upper bound for the potential effects of an optimized lane changing distribution on the capacity of weaving sections can be defined. The lower bound results from the conservative case where the reaction times associated to automated vehicles equals the one associated to conventional vehicles. It corresponds to the values of $E_{LC}(pr)$ for the simulation study conducted within this paper. On the contrary, the upper bound relates to $E_{LC}(pr)+E_{IN}(pr)$, including the combination effects obtained by decreasing the reaction time. Note that the value of the upper bound increases if the selected reaction time decreases. Nevertheless, the general trend still applies. Both bounds are illustrated in Figure 12. Based on the simulation study performed in this paper, we expect that the benefit of the optimization of the lane change distributions lies between the two bounds. This shows the potential of such optimization with AVT for this case.

The extent of the benefits of optimizing lane changes is influenced by other input parameters such as the ratio in the traffic stream which desires to change lanes, the length of the weaving section, etc. Nevertheless, the trends shown based on the input parameter configuration used here will still be valid. The simulation study shows a proof of concept of the proposed extension of the MHT for weaving sections.

6. Conclusion

This paper proposes a hybrid multi-class model to study the effects of automated vehicles on weaving sections, which has been rarely explored in the literature. Two aspects of automated vehicles are studied, i.e. the flexibility to control the lane change decision and the reduction in reaction times. The proposed model builds on the MHT, and extends it by considering multiple vehicle classes. Additionally, we modify the original MHT to model mandatory instead of discretionary lane changes and take the lane change distributions as a direct exogenous input. Apart from the fundamental diagram, the proposed model includes three calibration parameters, two more than the original MHT. It is shown that the proposed model successfully reproduces traffic states in the weaving section as well as the capacity drop phenomenon for a weaving section close to the city of Basel, Switzerland. Thus, the model is able to reproduce important traffic dynamics occurring during high demand in weaving sections.

Simulation is conducted to examine the effects of the two aforementioned aspects alone as well as their combination effects. Both aspects of automated vehicles are found to have substantial effects on the capacity.

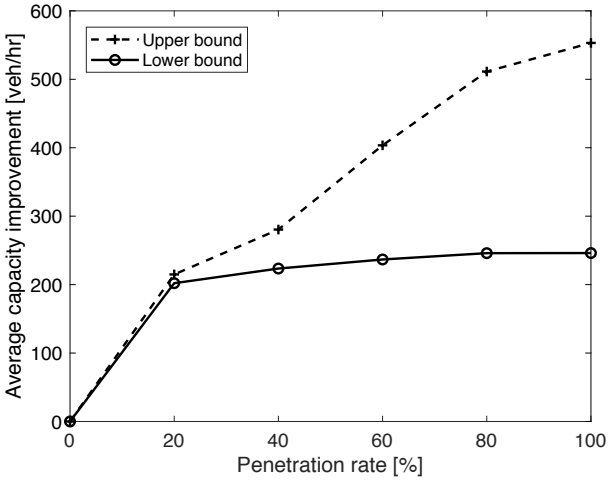

Figure 12: Upper and lower bound for capacity improvements by AVT.

For the lane change distribution, the analyses of different penetration rates show that the actual discharge rate can be increased with a growing share of automated vehicles in the traffic stream. The marginal effects are found to decrease with higher penetration rates. For the reduced reaction time, the results show a non-linear increase of the capacity of the simulated weaving section with a growing penetration rate. However, the capacity reduction, defined as the relative difference between the maximum theoretical capacity and the actual capacity increases. Lastly, both aspects are considered simultaneously. The simulation results show that the further increase of the capacity reduction in case of different reaction times for both vehicle classes can be mostly prevented with a quasi-optimal distribution of lane changes. Moreover, the analysis reveals that a positive combination effect exists for the simulated weaving section. This means that the additional capacity gained by considering both aspects together is higher than the sum of additional capacities resulting from each aspect considered separately.

It is concluded that the consideration of lower average reaction times due to automated vehicle technology leads to an underestimation of the capacity increase if automated vehicles can also be controlled. To sum up, the analysis of mixed traffic in weaving sections with the modified MHT shows the potential of controlling the desired lane change positions of automated vehicles in terms of increasing capacity. The model indicates a lower and an upper bound for the effects of AVT on the capacity of weaving sections.

Future research includes extensions to the modified MHT. Discretionary lane changes can be modeled in addition to mandatory ones. Furthermore, the effects of platoons of automated vehicles on the capacity could also be investigated. The results of the current study give insights on the optimum lane change distribution in weaving sections with respect to its capacity. This could be of guidance for a microscopic algorithm for the control of automated vehicles. The development of an optimization algorithm applicable for real time traffic control will further increase possible capacity gains.

References

Allen, R., Harwood, D., Chrstos, J., Glauz, W., 2000. The capability and enhancement of VDANL and TWOPAS for analyzing vehicle performance on upgrades and downgrades within IHSDM. Technical Report. Federal Highway Administration.

Björkman, M., Holmström, K., 2000. Global Optimization of Costly Nonconvex Functions Using Radial Basis Functions. Optimization and Engineering 1, 373–397. doi:10.1023/A:1011584207202.

Cassidy, M.J., Bertini, R.L., 1999. Some Traffic Features at Freeway Bottlenecks. Transportation Research Part B: Methodological 33, 25–42. doi:http://dx.doi.org/10.1016/S0191-2615(98)00023-X.

Cassidy, M.J., Rudjanakanoknad, J., 2005. Increasing the capacity of an isolated merge by metering its on-ramp. Transportation Research Part B: Methodological 39, 896–913. doi:10.1016/j.trb.2004.12.001, arXiv:9809069v1.

Chen, D., Ahn, S., 2018. Capacity-drop at extended bottlenecks: Merge, diverge, and weave. Transportation Research Part B:

Methodological 108, 1 – 20. URL: http://www.sciencedirect.com/science/article/pii/S0191261517306938, doi:https://doi.org/10.1016/j.trb.2017.12.006.

Chen, D., Ahn, S., Chitturi, M., Noyce, D.A., 2017. Towards vehicle automation: Roadway capacity formulation for traffic mixed with regular and automated vehicles. Transportation Research Part B: Methodological 100, 196 – 221. URL: http://www.sciencedirect.com/science/article/pii/S0191261516305471, doi:https://doi.org/10.1016/j.trb.2017.01.017.

Chung, K., Rudjanakanoknad, J., Cassidy, M.J., 2007. Relation between traffic density and capacity drop at three freeway bottlenecks. Transportation Research Part B: Methodological 41, 82–95. doi:10.1016/j.trb.2006.02.011.

Daamen, W., Loot, M., Hoogendoorn, S., 2010. Empirical analysis of merging behavior at freeway on-ramp. Transportation Research Record: Journal of the Transportation Research Board , 108–118.

Daganzo, C.F., Laval, J.A., 2005. On the numerical treatment of moving bottlenecks. Transportation Research Part B: Methodological 39, 31–46. doi:10.1016/j.trb.2004.02.003.

Friedrich, B., 2015. Verkehrliche Wirkung autonomer Fahrzeuge, in: Autonomes Fahren. Springer, pp. 331–350. doi:10.1007/978-3-662-45854-9.

Ge, Q., Ciuffo, B., Menendez, M., 2014. An Exploratory Study of Two Efficient Approaches for the Sensitivity Analysis of Computationally Expensive Traffic Simulation Models. IEEE Transactions on Intelligent Transportation Systems 15, 1288–1297. doi:10.1109/TITS.2014.2311161.

Ge, Q., Ciuffo, B., Menendez, M., 2015. Combining screening and metamodel-based methods: An efficient sequential approach for the sensitivity analysis of model outputs. Reliability Engineering & System Safety 134, 334–344. doi:https://doi.org/10.1016/j.ress.2014.08.009.

Ge, Q., Menendez, M., 2017. Extending Morris method for qualitative global sensitivity analysis of models with dependent inputs. Reliability Engineering & System Safety 162, 28–39. doi:10.1016/j.ress.2017.01.010.

Guler, S.I., Menendez, M., Meier, L., 2014. Using connected vehicle technology to improve the efficiency of intersections. Transportation Research Part C: Emerging Technologies 46, 121–131.

Gutmann, H.M., 2001. A Radial Basis Function Method for Global Optimization. Journal of Global Optimization 19, 201–227. doi:10.1023/A:1011255519438.

Hall, F.L., Agyemang-Duah, K., 1991. Freeway Capacity Drop and the Definition of Capacity. Transportation Research Record: Journal of the Transportation Research Board 1320, 91–98.

Hartmann, M., Motamedidehkordi, N., Krause, S., Hoffmann, S., Vortisch, P., Busch, F., 2017. Impact of automated vehicles on capacity of the german freeway network .

He, H., Menendez, M., 2016. Distribution and impacts of lane changes at a freeway weaving section: an empirical study, in: Transportation Research Board 95th Annual Meeting.

He, X., 2014. Simulation-Based Optimization of Transportation Systems: Theory, Surrogate Models, and Applications. Ph.D. thesis. University of Maryland.

Jin, W.L., 2010. A kinematic wave theory of lane-changing traffic flow. Transportation Research Part B: Methodological 44, 1001–1021. doi:10.1016/j.trb.2009.12.014, arXiv:0503036.

Kerner, B.S., 2002. Empirical macroscopic features of spatial-temporal traffic patterns at highway bottlenecks. Physical Review E - Statistical, Nonlinear, and Soft Matter Physics 65, 1–30. doi:10.1103/PhysRevE.65.046138.

Koehler, J., Owen, A., 1996. Computer experiments, in: Gosh, S., Rao, C. (Eds.), Handbook of Statistics, 13: Design and Analysis of Computer Experiments, pp. 261–308.

Laval, J., Cassidy, M., Daganzo, C., 2007. Impacts of lane changes at merge bottlenecks: a theory and strategies to maximize capacity. Traffic and Granular Flow'05 , 1–9doi:10.1007/978-3-540-47641-2_56.

Laval, J.A., Daganzo, C.F., 2003. A Hybrid Model of Traffic Flow: Impacts of Roadway Geometry on Capacity. TRB 2003 Annual Meeting CD-ROM. Submitted for publication. .

Laval, J.A., Daganzo, C.F., 2004. Multi-Lane Hybrid Traffic Flow Model: Quantifying the Impacts of Lane-Changing Maneuvers on Traffic Flow , 1–17.

Laval, J.A., Daganzo, C.F., 2006. Lane-changing in traffic streams. Transportation Research Part B: Methodological 40, 251–264. doi:10.1016/j.trb.2005.04.003.

Laval, J.A., Leclercq, L., 2008. Microscopic modeling of the relaxation phenomenon using a macroscopic lane-changing model. Transportation Research Part B: Methodological 42, 511–522. doi:10.1016/j.trb.2007.10.004.

Leclercq, L., Knoop, V., Marczak, F., Hoogendoorn, S., 2016a. Capacity Drops at Merges: New Analytical Investigations. Transportation Research Part C: Emerging Technologies 62, 171–181.

Leclercq, L., Laval, J.A., Chiabaut, N., 2011. Capacity drops at merges: An endogenous model. Transportation Research Part B: Methodological 45, 1302–1313. doi:10.1016/j.trb.2011.05.007.

Leclercq, L., Marczak, F., Knoop, V.L., Hoogendoorn, S.P., 2016b. Capacity drops at merges: analytical expressions for multilane freeways. Transportation Research Record: Journal of the Transportation Research Board , 1–9.

Lee, J., Cassidy, M.J., 2009. An Empirical and Theoretical Study of Freeway Weave Bottlenecks. California PATH program , 70.

Lee, J.H., 2008. Observations on Traffic Behavior in Freeway Weaving Bottlenecks: Empirical Study and Theoretical Modeling. Ph.D. thesis. University of California, Berkeley.

Levin, M.W., Boyles, S.D., 2016. A multiclass cell transmission model for shared human and autonomous vehicle roads. Transportation Research Part C: Emerging Technologies 62, 103–116. doi:10.1016/j.trc.2015.10.005.

Lighthill, M.J., Whitham, G.B., 1955. On Kinematic Waves. II. A Theory of Traffic Flow on Long Crowded Roads. Proceedings of the Royal Society A: Mathematical, Physical and Engineering Sciences 229, 317–345. doi:10.1098/rspa.1955.0089.

Majid Sarvi, M.K., 2010. Observing freeway ramp merging phenomena in congested traffic. Journal of Advanced Transportation 41, 145 – 170. doi:10.1002/atr.5670410203.

Marczak, F., Daamen, W., Buisson, C., 2014. Empirical analysis of lane changing behavior at a freeway weaving section, in: Transportation Research Board Annual Meeting, Paper, Citeseer. pp. 14–1097.
Marczak, F., Leclercq, L., Buisson, C., 2015. A Macroscopic Model for Freeway Weaving Sections. Computer-Aided Civil and Infrastructure Engineering 30, 464–477. doi:10.1111/mice.12119.
Menendez, M., 2006. An Analysis of HOV Lanes: Their Impact on Traffic. Ph.D. thesis. University of California, Berkeley.
Menendez, M., Daganzo, C.F., 2007. Effects of hov lanes on freeway bottlenecks. Transportation Research Part B: Methodological 41, 809–822.
Menendez, M., He, H., 2017. Final report on project WEAVE - Capacity and level of service for freeway weaving areas. Technical Report. Zurich.
Montgomery, D.C., 2017. Design and analysis of experiments. John wiley & sons.
Morris, M.D., Mitchell, T.J., 1995. Exploratory designs for computational experiments. Journal of statistical planning and inference 43, 381–402.
Müller, J., 2014a. Matsumoto code documentation .
Müller, J., 2014b. MATSuMoTo: The MATLAB Surrogate Model Toolbox For Computationally Expensive Black-Box Global Optimization Problems. arXiv preprint arXiv:1404.4261 arXiv:1404.4261.
Müller, J., Piché, R., 2011. Mixture surrogate models based on dempster-shafer theory for global optimization problems. Journal of Global Optimization 51, 79–104.
Müller, J., Shoemaker, C.A., 2014. Influence of ensemble surrogate models and sampling strategy on the solution quality of algorithms for computationally expensive black-box global optimization problems. Journal of Global Optimization 60, 123–144.
Müller, J., Shoemaker, C.A., Piché, R., 2013. So-mi: A surrogate model algorithm for computationally expensive nonlinear mixed-integer black-box global optimization problems. Computers & Operations Research 40, 1383–1400.
Müller, J., Shoemaker, C.A., Piché, R., 2014. So-i: a surrogate model algorithm for expensive nonlinear integer programming problems including global optimization applications. Journal of Global Optimization 59, 865–889.
National Highway Traffic Safety Administration, 2013. Preliminary Statement of Policy Concerning Automated Vehicles. Technical Report. National Highway Traffic Safety Administration.
Ngoduy, D., 2006. Derivation of Continuum Traffic Model for Weaving Sections on Freeways. Transportmetrica 2, 199–222. doi:10.1080/18128600608685662.
Oh, S., Yeo, H., 2012. Estimation of Capacity Drop in Highway Merging Sections. Transportation Research Record: Journal of the Transportation Research Board 2286, 111–121. doi:10.3141/2286-13.
Pan, T.L., Lam, W.H.K., Sumalee, A., Zhong, R.X., 2016. Modeling the impacts of mandatory and discretionary lane-changing maneuvers. Transportation Research Part C: Emerging Technologies 68, 403–424. doi:10.1016/j.trc.2016.05.002.
Regis, R.G., Shoemaker, C.A., 2005. Constrained global optimization of expensive black box functions using radial basis functions. Journal of Global Optimization 31, 153–171. doi:10.1007/s10898-004-0570-0.
Regis, R.G., Shoemaker, C.A., 2007. A Stochastic Radial Basis Function Method for the Global Optimization of Expensive Functions. European Journal of Operational Research 182, 514–535. doi:10.1016/j.ejor.2006.08.040.
Richards, P.I., 1956. Shock Waves on the Highway. Operations Research 4, 42–51. doi:10.1287/opre.4.1.42.
Spall, J.C., 1992. Multivariate stochastic approximation using a simultaneous perturbation gradient approximation. IEEE transactions on automatic control 37, 332–341.
Sulejic, D., Jiang, R., Sabar, N.R., Chung, E., 2017. Optimization of lane-changing distribution for a motorway weaving segment. Transportation Research Procedia 21, 227–239. doi:10.1016/j.trpro.2017.03.092.
Talebpour, A., Mahmassani, H.S., 2016. Influence of connected and autonomous vehicles on traffic flow stability and throughput. Transportation Research Part C: Emerging Technologies 71, 143–163. doi:10.1016/j.trc.2016.07.007.
Tanaka, S., Hasegawa, N., Iizuka, D., Nakamura, F., 2017. Evaluation of vehicle control algorithm to avoid conflicts in weaving sections under fully-controlled condition in urban expressway. Transportation Research Procedia 21, 199–207. doi:10.1016/j.trpro.2017.03.089.
Yang, K., Guler, S.I., Menendez, M., 2016. Isolated intersection control for various levels of vehicle technology: Conventional, connected, and automated vehicles. Transportation Research Part C: Emerging Technologies 72, 109–129. doi:10.1016/j.trc.2016.08.009.
Yang, K., Menendez, M., Guler, S.I., 2018. Implementing transit signal priority in a connected vehicle environment with and without bus stops. Transportmetrica B: Transport Dynamics doi:10.1080/21680566.2018.1434019.
Yuan, K., Knoop, V.L., Hoogendoorn, S.P., 2014. Capacity Drop: a Relation Between the Speed In Congestion And The Queue Discharge Rate. Transportation Research Record: Journal of the Transportation Research Board 2491, 72–80.
Zhou, L., Yan, G., Ou, J., 2013. Response Surface Method Based on Radial Basis Functions for Modeling Large-Scale Structures in Model Updating. Computer-Aided Civil and Infrastructure Engineering 28, 210–226. doi:10.1111/j.1467-8667.2012.00803.x.

Appendix A. Impact of reaction times under various penetration rates

One potential advantage of automated vehicles is that they typically have shorter reaction times than conventional vehicles. This leads to shorter headways and smaller required gaps for lane changing maneuvers, and thus an increased capacity and backward wave speed in the fundamental diagram.

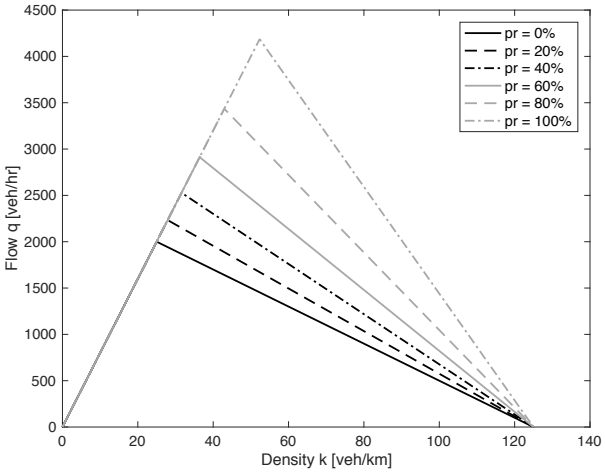

Figure A.13: Impact of reaction time differences on the fundamental diagram.

Levin and Boyles (2016) studied the impact of reaction time on the fundamental diagram under various penetration rates. Mathematically, the capacity for heterogeneous flows is described as follows. For more details regarding the derivation, please refer to Levin and Boyles (2016).

$$Q = u \frac{1}{u \sum_{m \in \mathcal{M}} \frac{k_m}{k_{tot}} t_{r,m} + \lambda} \tag{A.1}$$

The backward-wave speed is computed as

$$w = \frac{\lambda}{\sum_{m \in \mathcal{M}} \frac{k_m}{k_{tot}} t_{r,m}} \tag{A.2}$$

where u is the free flow speed, m index of the vehicle class, $\mathcal{M}$ the set of vehicle classes, $t_{r,m}$ the reaction time of vehicle class m, k_m the density of vehicle class m, k_{tot} the total density, and λ the average vehicle length.

With an increasing penetration rate, the reaction time associated to automated vehicles leads to a fundamental diagram with greater values for both the capacity and the backward wave speed. The fundamental diagram of each cell is adapted according to the proportion of automated vehicles in it (see Figure A.13).